Influences of bioapatite mineral and fibril structure on the mechanical properties of chicken bone during the laying period

Shujie Wang,[*] Yunxiao Hu,[†] Yiling Wu,[†] Yawen Liu,[*] Guoqing Liu,[*] Zhuojun Yan,[*] Qiao Li,[*] Zhenlei Zhou,[*,1] and Zhen Li[†,1]

[*]*College of Veterinary Medicine, Nanjing Agricultural University, Nanjing, Jiangsu 210095, China; and* [†]*College of Resources and Environmental Sciences, Nanjing Agricultural University, Nanjing, Jiangsu 210095, China*

ABSTRACT Laying hens suffer from osteoporosis during their laying period, which causes bone fragility and susceptibility to fracture. This study evaluated the changes of mechanical properties of their bones during the laying period (from 18 to 77 wk) by using nano-indentation, atomic force microscope, X-Ray diffraction, and Raman spectroscopy. Results indicated that the crystallite sizes of bioapatite in femur decreased significantly from 34.45 to 29.26 nm during aging from 18 to 49 wk. Then, the value increased to 37.79 nm at 77 wk. Despite the abundance in bone (usually >50 wt.%), bioapatite mineral content showed no continuous enhancement during aging. The fibrils demonstrated more regular and organized structure during the laying period. Meanwhile the elastic moduli (E) and hardness (H) of femur increased from 10.84 to 18.39 GPa and 43.79 to 97.21 Vickers respectively during this period. The changes in mechanical properties are hence tightly related to the structure of bone (composed of both collagen and mineral), rather than directly related to the mineralogical properties of bone bioapatite. This study addressed the importance of the interaction between collagen and bioapatite mineral during the laying period of hens by microscopic, physicochemical, and mechanical analysis.

Key words: laying period, laying hen, mechanical property, bioapatite mineral, fibril structure

2019 Poultry Science 98:6393–6399
http://dx.doi.org/10.3382/ps/pez474

INTRODUCTION

Bone typically consists of collagen fibrils and minerals, which have critical roles in its strength and stiffness (Viguet-Carrin et al., 2006). Mechanical properties of bone are likely to be influenced by egg laying in most avian species. In particular, at the expense of the more structural cortical bone, the available calcium during the laying period may favor the formation of "medullary bone" on the endosteal surface (Hurwitz, 1965; Dacke et al., 1993; Knott et al., 1995). This process provides a mineral source for eggshells. However, it could induce osteoporosis. Therefore, tracking the changes in mechanical properties during the laying period is of great importance in poultry science.

The biomechanical properties of bone depend on the quality and spatial arrangement of both collagen fibrils and minerals. Previous research has suggested that the mineral predominantly contributes to bone stiffness (Smith and Smith, 1976; Singer et al., 1995), whereas the quality of the collagen matrix may determine the toughness of bone (Burstein et al., 1975; Currey et al., 1997; Boskey et al., 1999; Zioupos et al., 1999). It was also shown that the dense hydroxylapatite (**HAp**) particles (the standard form of bioapatite) exhibit the trend of decreasing hardness with increasing crystallite size at micro/nano-meter scale (Ramesh et al., 2008; Mazaheri et al., 2009; Veljović et al., 2009), consistent with the classical Hall–Petch relation for large grained polycrystals. However, the studies of crystallite size determination of HAp hardness at micro/nano-meter scale are still scanty.

There are evidences that bioapatite (**BAp**) of bone is deposited almost exclusively within the collagen fibrils (Glimcher, 1959; White et al., 1977; Berthet-Colominas et al., 1979; Lee and Glimcher, 1991). Imaging the mineralized fibrils and structural relations inside bone is an indispensable step in elucidating the changes of bone BAp during the laying period. Therefore, a spatial resolution at nanometer scale is required. It has been reported that the atomic force microscope (**AFM**) was capable of elucidating the structure on the surface of bone at nanometer level. For example, AFM on bovine trabecular bone revealed a densely woven structure of collagen fibrils with a 67 nm banding pattern and densely packed mineral plates (Hassenkam et al., 2004). However, the changes in BAp crystallite size and structure during aging and egg laying cannot be elucidated solely by AFM. Structural studies by X-Ray

Received January 6, 2019.
Accepted July 31, 2019.
[1]Corresponding authors: lizhen@njau.edu.cn (ZL); zhouzl@njau.edu.cn (zz)

diffraction (**XRD**) may aid in elucidating the mineralogic nature of apatite, with particular emphasis on the lattice structure. Moreover, previous XRD studies on bone apatite of human iliac crest indicated a significant correlation of several crystallographic parameters (lattice data, crystallinity) in cortical and trabecular bone during aging (Handschin and Stern, 1992). These studies imply physicochemical and structural modifications of the bone BAp during aging in animals.

Bones of laying hens show heavy calcium loss and strong carbonate substitution during their laying period (Li et al., 2016). In addition, the sharply increased carbonate content during egg laying is different from a gradual elevation of carbonate content during aging. Gushi chicken is one of the most common local chicken breeds in China, which has been cultivated as both layer and meat chickens (Li et al., 2016). The Gushi layers have relatively large egg size and strong resistance to disease. Additionally, Gushi layers reach sexual maturity around 18 wk (**w**) of age, reach peak of egg laying at about 49 wk, and significantly reduce laying at ∼77 wk. Therefore, the bone of Gushi layers, bearing intense mineral composition changes, is the ideal material for tracing crystallite size and collagen fibril structure in hens.

The aim of this study was to combine AFM, XRD, and nano-indentation to investigate the mineralogical changes of the femur (with typical BAp for mineralogical study in laying hens) during the laying period of hens. Gushi layers were selected as the experimental animal.

MATERIALS AND METHODS

Sample Preparation

A total of 300 laying hens were cultured cage free and feed with the diet according to the nutrition requirement of the flock, which contains 11.55 MJ/kg of metabolizable energy, 16.5 wt.% crude protein, 3.63 wt.% Ca, 0.4 wt.% P, 0.35 wt.% methionine, and 0.95 wt.% lysine. A total of 8 hens from the 300 laying hens (Gushi layer, local strains) were randomly selected and killed at each of 11 wk (before sexual maturity), 18 wk (sexual maturity), 49 wk (peak time of egg laying), and 77 wk (end of laying) of age (the same batch of laying hens as in our previous study) (Li et al., 2016). The right femoral bones were collected and cleaned of all adherent tissue (the left humeri and femoral bones were used in our previous study). The mid-diaphyseal segments (∼2 cm long area was selected) were collected from each right femur using a precision saw (Isomet 2000, Buehler, Lake Bluff, IL). They were cleaned and dried following our previous protocol (Li et al., 2016). All animal work was performed according to the Guidelines for Experimental Animals of the Ministry of Science and Technology, and the protocols were approved by the Experimental Animal Welfare and Ethics Committee of Nanjing Agricultural University (#NJAU-Poult-2014,003).

Instrumentation

Mineralogical characterization of the crystallization products was examined by XRD using a Bruker D8 diffractometer (Cu-Ka; 40 kV; 40 mA; scanned from 10 to 60° at a speed of 0.02°/s). The lattice parameters were then calculated by General Structure Analysis System (**GSAS**, Los Alamos National Laboratory).

Images of surface topography were recorded in air, at room temperature, by using a commercial AFM device (Dimension Icon, Bruker) at a tapping mode. An aluminum reflex coated silicon cantilever probe with a cone tip was applied (Tap 150AI-G, Budget Sensors, Innovative Solutions Bulgaria Ltd., Sofia, Bulgaria).

The contents of bone mineral and collagen matrix were measured by a Raman microprobe (HR 800 Evolution, Horriba, Inc.). Raman spectroscopy was performed on the surface of the femoral shaft (4 × 4 s per spot, 400 to 4000 cm^{-1}, 532 nm excitation, 50% laser power). Raman analysis on each sample was performed three times (on 3 different spots). The peak positions were calibrated by silicon wafer (520.5/cm).

A CSM NHTX nano-indenter was used to measure the hardness with a Berkovich indenter and a maximum load of 20 mN maintained for 10 s. The load and unload rates were 40 mN/min. Each sample was indented 90 times in a 10 × 9 matrix and the distance between the neighboring indents was 30 mm.

Statistical Analysis

All data are presented as means ± standard deviation. The differences among the groups were determined by one-way analysis of variance (ANOVA, Dunnet's T3). Significant differences were accepted if $P < 0.05$.

RESULTS

Atomic Force Microscope

Figure 1 shows AFM amplitude images at 10 × 10 μm scale on the exterior surface of laying hen femurs at four stages of age. Collagen fibrils are the dominant feature and have preferred orientation under AFM. At 11 wk, the surface of the bone is relatively disordered with scattered protrusions around and the fibers are not well organized. Although single fibrils cannot be observed, the fibrils at 18 wk are better organized compared with those at 11 wk (Figure 1A and B). The bone surface at 49 wk has no evident change compared with that for 18 wk (Figure 1C). At 77 wk, the surface is more rugged (see the evident elevation of fibril height), and the fibrils display a denser structure (Figure 1D).

Higher resolution images (2 × 2 μm scale) of the surface of the femurs are shown in Figure 2. The ultrastructure of the surface reveals detailed information about the exterior of mineralized collagen fibrils. On the surface of 11 wk bone, there are some particle-like protrusions on top of the fibrils (Figure 2A). The individual fibrils cannot be easily distinguished as they

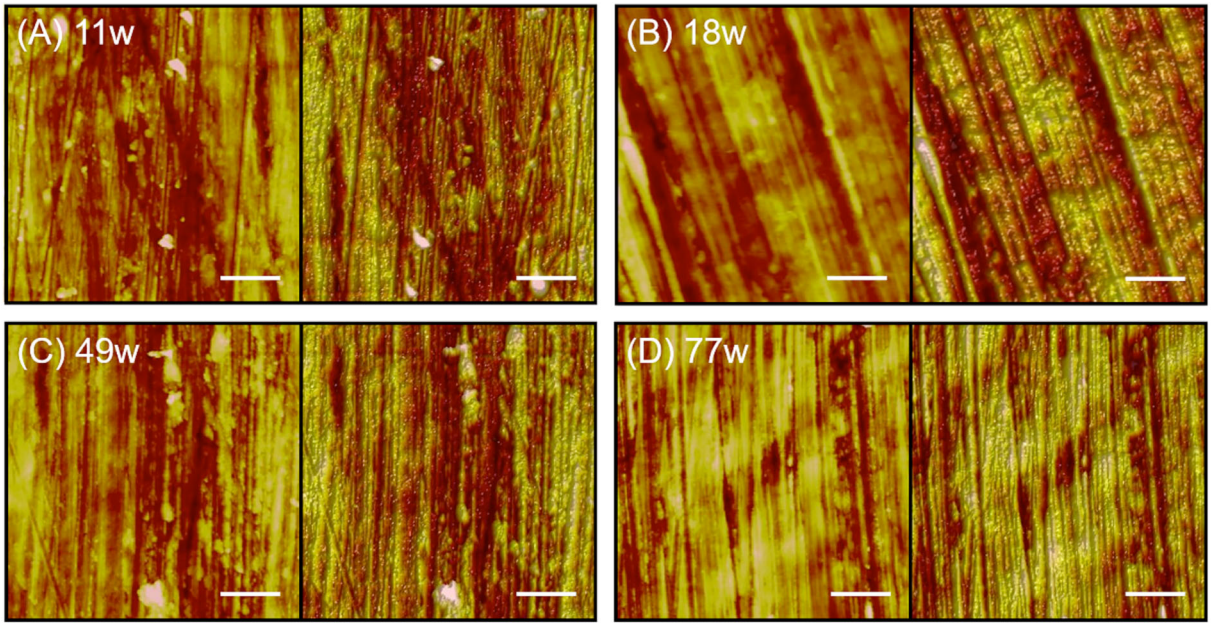

Figure 1. 10 × 10 μm AFM amplitude images (left) and typical AFM height images (right) on the surface of hens' femur at 4 different growing stages. The fibrils are better organized at 18 than 11 wk. From 49 to 77 wk, the fibrils display a denser structure. Scale bar = 2 μm for all the images.

are lying tightly or intertwined with their neighboring fibrils. The morphology of fibrils in the femur becomes more regular and structured during aging (Figure 2B). The widths of the fibrils at 49 and 77 wk are larger than those of 11 and 18 wk and many single fibrils could be well resolved (Figure 2C and D). However, there are large voids within the fibrillar fabric at 49 and 77 wk. Moreover, from 11 to 77 wk, 2 height profiles extracted from each AFM image gradually change to mutually match, confirming the improved organization.

XRD and Lattice Calculation

XRD was applied to examine the mineralogy of BAp in the femur. The basic lattice parameter and crystallite size estimates (by GSAS) are shown in Table 1. Data were refined for instrument effects and the Scherrer equation used with the full width at half intensity to estimate the maximal crystallite sizes (Kuhn et al., 2008).

The lattice parameters of BAp measured by XRD are close to the HAp. Pure HAp is hexagonal with c = 0.6875 nm and a = 0.9416 nm (Heijligers et al., 1979). The results of XRD show that the lattice c parameter of BAp varies between 0.6877 and 0.6922 nm at different ages. Meanwhile, the lattice a parameter varies between 0.9328 and 0.9449 nm. The lattice parameters indicate that the crystallites became elongated from 18 (sexual maturity) to 49 wk (peak time of egg laying). However, the maximal crystallite size calculated using the Scherrer equation shows that the mineral has smaller crystallites at 49 wk than those at the other three age stages.

Raman Spectroscopy

The ~1070 cm^{-1} peak represents a combination of the $\nu 3$ vibrational mode of PO_4^{3-} and the $\nu 1$ C-O stretching vibration of CO_3^{2-} (Li et al., 2015). An envelope of peaks centered at ~2940 cm^{-1} is assigned to C-H stretching vibrations in multiple organic materials, e.g., collagen or non-collagenous proteins (Penel et al., 2005). The intensity of Raman peaks can be applied to estimate the relative contents of the corresponding compounds (Li and Pasteris, 2014b).

Figure 3 shows the 1070 cm^{-1} (indicating the carbonate contents) and 2940 cm^{-1} peaks (indicating the organic matrix) of femur at four growing stages. All the spectra are normalized to the intensity of the 960 cm^{-1} peak (the dominant peak of BAp phase). The intensity of the 1070 cm^{-1} peak increases dramatically from 11 to 49 wk and then remains stable until 77 wk. Additionally, the intensity of the 2940 cm^{-1} peak decreases from 11 to 49 wk, which indicates that the contents of organic matter decrease in the femur or the degree of bone mineralization relatively raises during this period. The Raman results are consistent with the above results of BAp by XRD and GSAS, i.e., an evident mineralogical change within 11 to 49 wk.

Nano-indentation

Four groups of elastic moduli (**E**) and nano-indentation hardness (**H**) of femur were obtained through load–displacement curves (Table 2). The E reflects the intrinsic stiffness or rigidity of bone. High E might suggest bone to be more rigid and less pliable, whereas low E may indicate bone to be more pliable and less mineralized (Turner and Burr, 1993). The

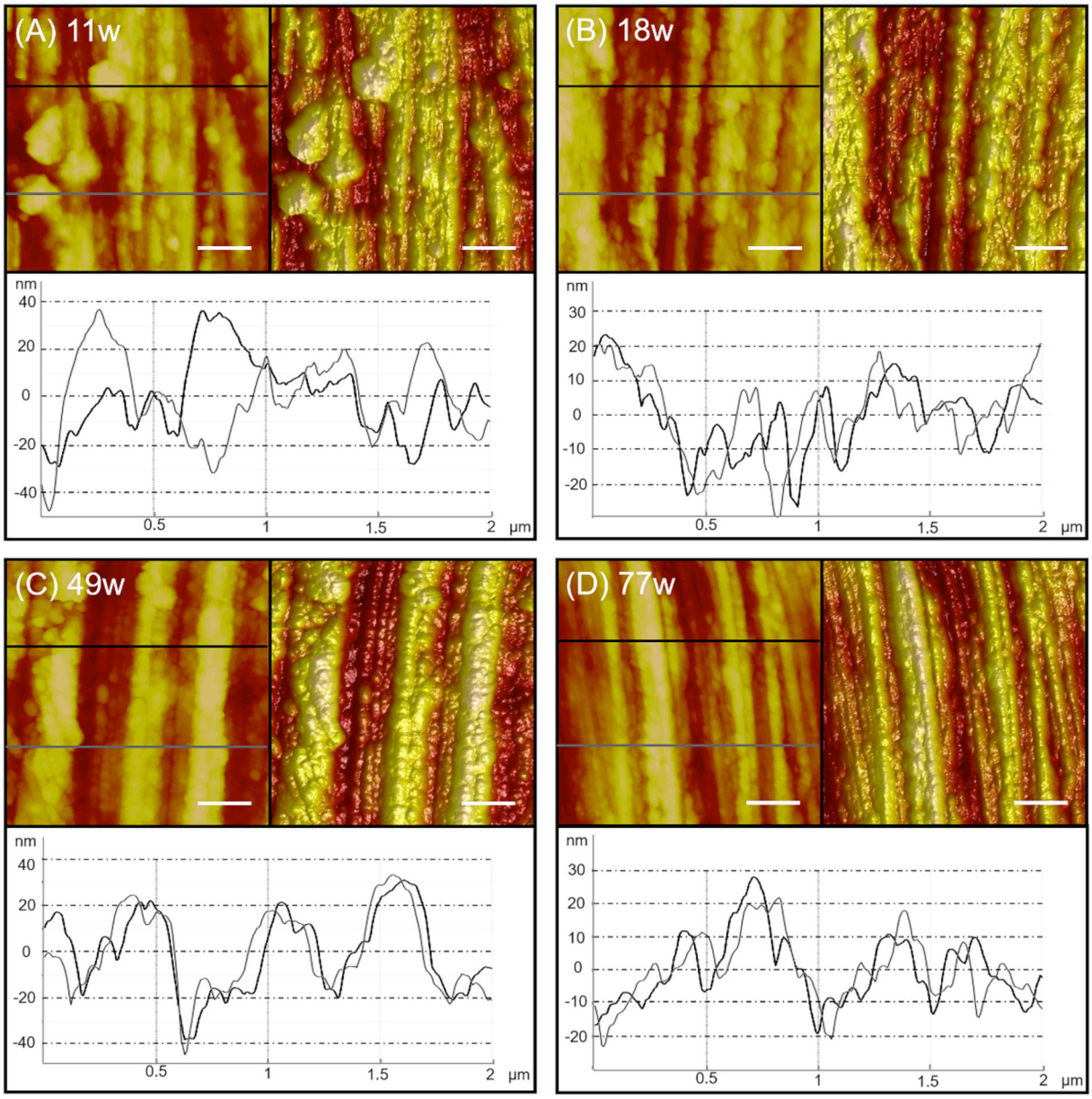

Figure 2. 2 × 2 μm AFM amplitude images (left) and typical AFM height images (right) on the surface of hens' femur at 4 different growing stages. Two height profiles extracted from the AFM image (marked by the black and gray lines) are indicated below each image. On the surface of 11 wk bone, there are some particle-like protrusions on top of the fibrils. The morphology of fibrils in the femur becomes more regular and structured from 11 to 77 wk. Scale bar = 0.4 μm for all the images.

Table 1. Calculation of crystallite sizes of BAp in hens' femur by GSAS based on XRD data.

	Lattice parameters (nm)		
Age	*a*	*c*	Size (nm)
11 wk	0.9431 (6)	0.6887 (62)	35.16
18 wk	0.9449 (5)	0.6877 (35)	34.45
49 wk	0.9438 (36)	0.6922 (49)	29.26
77 wk	0.9328 (48)	0.6918 (6)	37.79

results indicate that the average E and H responses of femur vary dramatically during aging (from 11 to 77 wk). The average E and H values decrease significantly from 13.45 GPa and 79.14 Vickers at 11 wk to 10.84 GPa and 43.79 Vickers at 18 wk, respectively. However, the average E and H of the hens' femurs increase during aging after 18 wk. Then, the values increase slightly to 15.54 GPa and 51.65 Vickers at 49 wk. However, the hardness of the femur at 49 wk is still significantly lower than that at 11 wk. The 77 wk femur has the highest E and H values (18.39 GPa and 97.21 Vickers) as compared to the other ages. This is also consistent with previous results, i.e., the peak of the egg laying period (from 18 to 49 wk) weakens the enhancement of bone quality due to aging (Li et al., 2016).

DISCUSSION

Cage layers exhibit a high incidence of bone problems including osteoporosis, bone weakness, deformity,

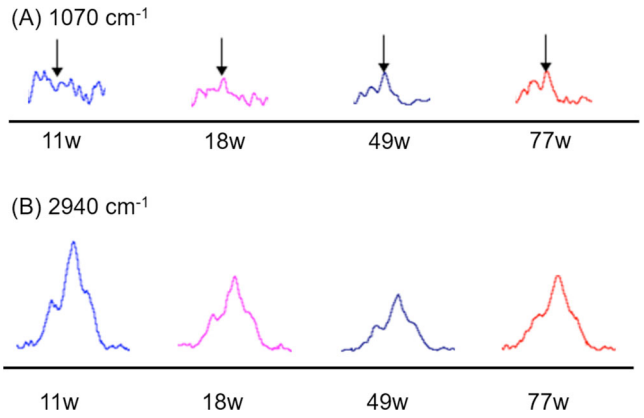

Figure 3. The intensities of 1070 and 2940 cm^{-1} peaks from 11 to 77 wk. The spectra were normalized to the intensity of the 960 cm^{-1} peak. The spectra were modified based on Figure 1 and 2 in Li *et al.*, 2016. The intensity of the 1070 cm^{-1} peak increases dramatically from 11 to 49 wk, while the intensity of the 2940 cm^{-1} peak decreases from 11 to 49 wk.

Table 2. Average elastic moduli (E) and hardness (H) of femur at various ages.

Age	E (GPa)	H (Vickers)
11 wk	$13.45^{a} \pm 0.63$	$79.14^{a} \pm 17.08$
18 wk	$10.84^{b} \pm 0.68$	$43.79^{b} \pm 5.62$
49 wk	$15.54^{c} \pm 1.37$	$51.65^{b} \pm 6.74$
77 wk	$18.39^{d} \pm 1.45$	$97.21^{a} \pm 12.84$

[a-d]no common superscripts within the column of each classification are significantly ($P < 0.05$) different.

Table 3. A summary of crystallite sizes of bone BAp using different analytical methods in previous literature.

Analytical methods	Crystal dimensions
TEM[a]	27.3 nm × 15.6 nm
XRD[b]	27–36 nm long
SAXS and WAXS[c]	34.5 nm × 16 nm × 2.8 nm
SAXS and TEM[d]	30 nm × 20 nm × 1.5–2 nm
AFM[e]	9–12 nm × 6–10 nm ×<2 nm

[a](Kim et al., 1995).
[b](Hanschin and Stern, 1995).
[c](Turunen et al., 2016).
[d](Burger et al., 2008).
[e](Eppell et al., 2001; Tong et al., 2003).

and breakage, which seriously influence hen welfare and economic efficiency. Therefore, it is essential to investigate the changes in bone during the laying period to better understand the relationship among mechanical properties, bone minerals and fibril structure.

BAp has a representative formula $(Ca, Mg, Na)_{10-x}[(PO_4)_{6-x}(CO_3)_x](OH)_{2-x}$, which is the primary component (50 to 60 wt.%) of bone (Elliott, 2002; Glimcher, 2006; Pasteris et al., 2014; Li and Pasteris, 2014a). It is formed within the collagen template after fast primary and protracted secondary mineralization stages. Described as plate- or needle-shaped in some literature (Dufrêne, 2003), the sizes of mineral crystallites vary significantly depending on the analytical technique (see Table 3). However, the changes in mineral crystallites during the laying period of hens are still unclear.

The morphology of the fibril structure varies with age, especially from the sexual maturity of layers to the peak of egg laying period (from 18 to 49 wk). Fibrils become thicker and the spacing between fibrils is elevated. This may be the result of bone maturity, which affects mineralization and collagen crosslinks (Knott and Bailey, 1998). In intensive livestock operations, bone development of fast-growing poultry may not exactly coincide with overall growth (Rath et al., 2000). The laying hens in this study are likely to reach bone maturity after 18 wk. Furthermore, the changes in fibrils may also be related to the continuous mineralization of bone. The deposition of minerals is thought to occur in spaces between collagen molecules in the pore and overlap zones of the fibrils (Landis et al., 1991; Tong et al., 2003). However, the volume available in the intermolecular region is considerably less than the volume of the minerals located in this space, so the deposition of minerals could cause considerable distortion of the fibril and/or collagen molecules (Katz and Li, 1973).

The changes in lattice parameters of bone mineral during aging, estimated by XRD, are consistent with previous studies, i.e., carbonate substitution led to a decline of a lattice constant, whereas the lattice parameter along the crystal *c*-axis increased with carbonate substitution (Deymier et al., 2017). In addition, studies on bovine bone have indicated an increase in crystallite size during aging (Kuhn et al., 2008). However, the crystallite size decreased from 18 to 49 wk based on XRD and GSAS modeling. BAp crystallite size and shape in bone are controlled via physical confinement by the fibrillar structure or chemical interactions with surrounding proteins and organic moieties. Egg-laying hens usually undergo heavy calcium loss and show strong carbonate substitution during their laying period. The smaller crystal particle allows the bone to present more surface area for effective dissolution, which contributes to the high requirements of Ca for egg shells. Furthermore, the smallest crystallite size in 49 wk femur may be conducive to its deposition in the narrow intermolecular region.

The results of nanoindentation show the growing trend of both E and H during aging. However, the 11 wk femurs have higher E and H compared to 18 wk. This is consistent with previous research, i.e., the bone of younger chickens is strong but fragile due to low collagen crosslinks and high mineral content (Mccoy et al., 1996). Additionally, several previous studies have investigated the effects of aging on the mechanical properties of normal bones from various species. There are still debates on changes of mechanical properties during aging. Some nanoindentation studies indicated both E and H increased during aging (Isaksson et al., 2010; Feng et al., 2012), whereas some literature demonstrated no significant change in E with increasing age (Hoffler et al., 2000; Rho et al., 2002). Moreover, it was also proposed that a significant decrease could occur in bone toughness and E (Ferguson et al., 2003; Akkus et al., 2004). These contradictory results are probably due to the

uncertainty or sample difference at the microscale structure. We confirmed that the E and H of bone increase during aging (from 11 wk to 77 wk) in laying hens, which indicates bone to be more rigid and less ductile. However, the changes of the sizes of BAp crystallites are not as evident as the values of E and H. It is possible that the mechanical property of layer bone may be related mainly to the structure of the fibrils, which are composed of collagen and minerals, rather than the crystallite size of bone BAp. The roles of minerals are hence over-estimated.

A typical bone contains ∼50 wt.% mineral and ∼30 wt.% organic material (Glimcher, 2006). Collagen–mineral structure makes bone a viscoelastic material and enables bone to continually adapt to changes in its physiologic or mechanical environment. The mechanical properties of bone depend mainly on the amount of bone mineral, its architecture, and also on the intrinsic properties of the mineral and organic matrix (Wang et al., 2002). These properties are critical for production performance of layers. However, the laying hen is the species that suffers most from osteoporosis due to the mineral loss throughout the laying period. Therefore, this study combined bone mineral, collagen structure, and mechanical properties to elucidate the changes in bone of layers during the laying period. The results will contribute to avoiding fragility and susceptibility to fracture in poultry farming.

In summary, the degree of mineralization in the femur increases from 18 to 49 wk, which may be a carbonate-compensated mineralization. Furthermore, bone mineralization may be responsible for the change of fibril structure, which become more regular and structured during aging. In addition, the elastic moduli (E) and hardness (H) of the femur increase during the laying period. However, the maximum crystallite size of bone BAp decreases sharply from 18 to 49 wk. Therefore, the mechanical properties of bone may be mainly related to the structure of the fibrils, which are composed of collagen and minerals, rather than directly related to the crystallite size of bone BAp.

ACKNOWLEDGMENTS

This work was supported by the National Natural Science Foundation of China (No. 31572579). This work was also partially supported by the Fundamental Research Funds for the Central Universities (No. KYZ201712) and Program for Student Innovation Through Research and Training (No. 1713C30). We thank Zhijun Wang for sample collection. We also thank Professor Yuanfeng Cai at Nanjing University for the assistance in GSAS modeling.

REFERENCES

Akkus, O., F. Adar, and M. B. Schaffler. 2004. Age-related changes in physicochemical properties of mineral crystals are related to impaired mechanical function of cortical bone. Bone. 34:443–453.

Berthet-Colominas, C., A. Miller, and S. W. White. 1979. Structural study of the calcifying collagen in turkey leg tendons. J. Mol. Biol. 134:431–445.

Boskey, A., T. Wright, and R. Blank. 1999. Collagen and bone strength. J. Bone. Miner Res. 14:330–335.

Burger, C., H. W. Zhou, H. Wang, I. Sics, B. S. Hsiao, B. Chu, L. Graham, and M. J. Glimcher. 2008. Lateral packing of mineral crystals in bone collagen fibrils. Biophys. J. 95:1985–1992.

Burstein, A. H., J. Zika, K. Heiple, and L. Klein. 1975. Contribution of collagen and mineral to the elastic-plastic properties of bone. J. Bone. Joint. Surg. Am. 57:956–961.

Currey, J. D., J. Foreman, I. Laketić, J. Mitchell, D. E. Pegg, and G. C. Reilly. 1997. Effects of ionizing radiation on the mechanical properties of human bone. J. Orthop Res. 15:111–117.

Dacke, C. G., S. Arkle, D. J. Cook, I. M. Wormstone, S. Jones, M. Zaidi, and Z. A. Bascal. 1993. Medullary bone and avian calcium regulation. J. exp.biol. 184:63–88.

Deymier, A. C., A. K. Nair, B. Depalle, Z. Qin, K. Arcot, C. Drouet, C. H. Yoder, M. J. Buehler, S. Thomopoulos, and G. M. Genin. 2017. Protein-free formation of bone-like apatite: New insights into the key role of carbonation. Biomaterials. 127:75–88.

Dufrêne, Y. F. 2003. Recent progress in the application of atomic force microscopy imaging and force spectroscopy to microbiology. Curr. Opin. Microbiol. 6:317–323.

Elliott, J. C. 2002. Calcium phosphate biominerals. Rev. Mineral. Geochem. 48:427–453.

Eppell, S. J., W. Tong, J. L. Katz, L. Kuhn, and M. J. Glimcher. 2001. Shape and size of isolated bone mineralites measured using atomic force microscopy. J. Orthop Res. 19:1027–1034.

Feng, L., M. Chittenden, J. Schirer, M. Dickinson, and I. Jasiuk. 2012. Mechanical properties of porcine femoral cortical bone measured by nanoindentation. J. Biomech. 45:1775–1782.

Ferguson, V. L., R. A. Ayers, T. A. Bateman, and S. J. Simske. 2003. Bone development and age-related bone loss in male C57BL/6 J mice. Bone. 33:387–398.

Glimcher, M. J. 1959. Molecular biology of mineralized tissues with particular reference to bone. Rev. Mod. Phys. 31:359–393.

Glimcher, M. J. 2006. Bone: nature of the calcium phosphate crystals and cellular, structural, and physical chemical mechanisms in their formation. Rev. Mineral. Geochem. 64:223–282.

Hanschin, R. G., and W. B. Stern. 1995. X-ray diffraction studies on the lattice perfection of human bone apatite (Crista iliaca). Bone. 16:355S.

Handschin, R. G., and W. B. Stern. 1992. Crystallographic lattice refinement of human bone. Calcif. Tissue. Int. 51:111–120.

Hassenkam, T., G. E. Fantner, J. A. Cutroni, J. C. Weaver, D. E. Morse, and P. K. Hansma. 2004. High-resolution AFM imaging of intact and fractured trabecular bone. Bone. 35:4–10.

Heijligers, H. J. M., F. C. M. Driessens, and R. M. H. Verbeeck. 1979. Lattice parameters and cation distribution of solid solutions of calcium and strontium hydroxyapatite. Calcif. Tissue. Int. 29:127–131.

Hoffler, C., K. Moore, K. Kozloff, P. Zysset, and S. A. Goldstein. 2000. Age, gender, and bone lamellae elastic moduli. J. Orthop Res. 18:432–437.

Hurwitz, S. 1965. Calcium turnover in different bone segments of laying fowl. Am. J. Physiol. 208:203–207.

Isaksson, H., M. Malkiewicz, R. Nowak, H. J. Helminen, and J. S. Jurvelin. 2010. Rabbit cortical bone tissue increases its elastic stiffness but becomes less viscoelastic with age. Bone. 47:1030–1038.

Katz, E. P., and S. T. Li. 1973. Structure and function of bone collagen fibrils. J. Mol. Biol. 80:1–15.

Kim, H. M., C. Rey, and M. J. Glimcher. 1995. Isolation of calcium-phosphate crystals of bone by non-aqueous methods at low temperature. J. Bone. Miner Res. 10:1589–1601.

Knott, L., and A. J. Bailey. 1998. Collagen cross-links in mineralizing tissues: a review of their chemistry, function, and clinical relevance. Bone. 22:181–187.

Knott, L., C. C. Whitehead, R. H. Fleming, and A. J. Bailey. 1995. Biochemical changes in the collagenous matrix of osteoporotic avian bone. Biophys. J. 310:1045–1051.

Kuhn, L. T., M. D. Grynpas, C. C. Rey, Y. Wu, J. L. Ackerman, and M. J. Glimcher. 2008. A comparison of the physical and chemical

differences between cancellous and cortical bovine bone mineral at two ages. Calcif. Tissue. Int. 83:146–154.

Landis, W. J., J. Moradian-Oldak, and S. Weiner. 1991. Topographic imaging of mineral and collagen in the calcifying turkey tendon. Connect. Tissue Res. 25:181–196.

Lee, D. D., and M. J. Glimcher. 1991. Three-dimensional spatial relationship between the collagen fibrils and the inorganic calcium phosphate crystals of pickerel (Americanus americanus) and herring (Clupea harengus) bone. J. Mol. Biol. 217:487–501.

Li, Z., Q. Li, S. J. Wang, L. Zhang, J. Y. Qiu, Y. Wu, and Z. L. Zhou. 2016. Rapid increase of carbonate in cortical bones of hens during laying period. Poult. Sci. 95:2889–2894.

Li, Z., S. P. Wu, and C. L. Ye. 2015. Temperature-related changes of bioapatite based on hypermineralized dolphin's bulla. J. Raman Spectros. 46:964–968.

Li, Z., and J. D. Pasteris. 2014a. Chemistry of bone mineral, based on the hypermineralized rostrum of the beaked whale Mesoplodon densirostris. Am. Mineral. 99:645–653.

Li, Z., and J. D. Pasteris. 2014b. Tracing the pathway of compositional changes in bone mineral with age: Preliminary study of bioapatite aging in hypermineralized dolphin's bulla. Biochim. Biophys. Acta. 1840:2331–2339.

Mazaheri, M., M. Haghighatzadeh, A. Zahedi, and S. Sadrnezhaad. 2009. Effect of a novel sintering process on mechanical properties of hydroxyapatite ceramics. J. Alloy. Compd. 471:180–184.

Mccoy, M. A., G. A. Reilly, and D. J. Kilpatrick. 1996. Density and breaking strength of bones of mortalities among caged layers. Res. Vet. Sci. 60:185–186.

Pasteris, J. D., C. H. Yoder, and B. Wopenka. 2014. Molecular water in nominally unhydrated carbonated hydroxylapatite: The key to a better understanding of bone mineral. Am. Mineral. 99:16–27.

Penel, G., C. Delfosse, M. Descamps, and G. Leroy. 2005. Composition of bone and apatitic biomaterials as revealed by intravital Raman microspectroscopy. Bone. 36:893–901.

Ramesh, S., C. Y. Tan, S. B. Bhaduri, W. D. Teng, and I. Sopyan. 2008. Densification behaviour of nanocrystalline hydroxyapatite bioceramics. J. Mater. Process. Tech. 206:221–230.

Rath, N., G. Huff, W. Huff, and J. Balog. 2000. Factors regulating bone maturity and strength in poultry. Poult. Sci. 79:1024–1032.

Rho, J. Y., P. Zioupos, J. D. Currey, and G. M. Pharr. 2002. Microstructural elasticity and regional heterogeneity in human femoral bone of various ages examined by nano-indentation. J. Biomech. 35:189–198.

Singer, K., S. Edmondston, R. Day, P. Breidahl, and R. Price. 1995. Prediction of thoracic and lumbar vertebral body compressive strength: correlations with bone mineral density and vertebral region. Bone. 17:167–174.

Smith, C., and D. Smith. 1976. Relations between age, mineral density and mechanical properties of human femoral compacta. Acta. Orthop. Scand. 47:496–502.

Tong, W., M. J. Glimcher, J. L. Katz, L. Kuhn, and S. J. Eppell. 2003. Size and shape of mineralites in young bovine bone measured by atomic force microscopy. Calcif. Tissue. Int. 72:592–598.

Turner, C. H., and D. B. Burr. 1993. Basic biomechanical measurements of bone: a tutorial. Bone. 14:595–608.

Turunen, M. J., J. D. Kaspersen, U. Olsson, M. Guizar-Sicairos, M. Bech, F. Schaff, M. Tägil, J. S. Jurvelin, and H. Isaksson. 2016. Bone mineral crystal size and organization vary across mature rat bone cortex. J. Struct. Biol. 195:337–344.

Veljović, D., B. Jokić, R. Petrović, E. Palcevskis, A. Dindune, I. Mihailescu, and D. Janaćković. 2009. Processing of dense nanostructured HAp ceramics by sintering and hot pressing. Ceram. Int. 35:1407–1413.

Viguet-Carrin, S., P. Garnero, and P. D. Delmas. 2006. The role of collagen in bone strength. Osteoporos. Int. 17:319–336.

Wang, X., X. Shen, X. Li, and A. C. Mauli. 2002. Age-related changes in the collagen network and toughness of bone. Bone. 31:1–7.

White, S. W., D. J. Hulmes, A. Miller, and P. A. Timmins. 1977. Collagen-mineral axial relationship in calcified turkey leg tendon by X-ray and neutron diffraction. Nature. 266:421–425.

Zioupos, P., J. Currey, and A. Hamer. 1999. The role of collagen in the declining mechanical properties of aging human cortical bone. J. Biomed. Mater Res. 45:108–116.